Phosphines Modulating the Catalytic Silane Activation on Nickel-Cobalt Nanoparticles, Tentatively Attributed to Frustrated Lewis Pairs in Colloidal Solution

Alberto Palazzolo,[1] Sophie Carenco,[1,*]

Sorbonne Université, CNRS, Collège de France, Laboratoire de Chimie de la Matière Condensée de Paris, 4 place Jussieu, 75005 Paris, France

Supporting Information available

ABSTRACT: The discovery of Frustrated Lewis Pairs (FLPs) represented a major breakthrough in modern organic chemistry, allowing the transition metal-free activation of chemical bonds in mild conditions. Consequently, FLP chemistry involving molecular Lewis acids and Lewis bases has witnessed an impressive advancement in the last decade. Nevertheless, the range of viable catalytic reactions are limited, due to the formation of too stable adducts between the reaction substrate and the Lewis acid/base couple and to the high distance between catalytic sites borne by separated molecular pairs in solution. In contrast with this, traditional heterogeneous catalysts made of transition metal nanoparticles present adjacent active sites, although they usually require harsher conditions to be activated. The design of FLP on metallic nanoparticles could allow the activation of small molecules in milder conditions. Herein we propose the concept of *NanoFLP* in colloidal solution where one partner is a phosphine Lewis base and the other is the Lewis acid surface of a NiCo nanoparticle. We attempt to apply this concept to the hydrosilylative reduction of benzaldehyde. While a classical surface organometallic path through the oxidative addition of the silane on the sole metal center cannot be disproved at this stage, the reaction requires the presence of at least 5 mol% phosphine in conjunction with the NiCo nanoparticles, which represent a tenfold excess of phosphines *vs.* metal surface atoms, a situation that should disfavor the presence of free metal sites apt to perform the oxidative addition. We identify a correlation between the Tolman cone angle and the silane conversion, consistent with both mechanisms, however, we found no clear correlation between the Tolman electronic parameter and the reaction outcome. The influence of the silane bulkiness was also investigated and a less bulky phosphine was required for the reaction to work with a bulkier silane. Structural analyses evidenced that the nanoparticles are not altered during the reaction, which led us to propose the formation of a *NanoFLP* as a transient species in solution.

Nowadays, intermolecular Frustrated Lewis Pairs (FLPs) have become an established technology for the activation of several chemical bonds, such as H–H, C=O, or S=O.[1] Bulky Lewis acid and base molecules form a frustrated Lewis adduct as a result of two opposite forces: a strong acid-base interaction and a strong steric hindrance. In solution, the two compounds can be mostly associated as a weak adduct, or separately solvated, i.e. dissociated. The insertion of a small molecule (eg. H_2, CO_2, SO_2) in the vicinity of the Lewis acid and base moieties drives the formation of a reactive intermediate, with a low activation energy for the cleavage of the bond.[2]

FLPs relying on two molecular partners have been thoroughly studied in the last decade. In these species, the mobility of the acid and base partner in solution allows the acid-base distance to self-adjust in the course of the reaction. However, they suffer for a number of limitations. First, the strength of the Lewis acidity and the bulkiness of the site cannot be independently tuned because they are governed by the same substituents. Second, molecular FLPs present only one active site, which requires the stability of the intermediate adduct to be weak enough in order not to break the catalytic cycle. Moreover, large-scale applicability of homogenous FLPs catalysts remains limited because of the use of molecular species hard to purify. Taking advantage of this technology in the field of heterogeneous catalysis appears thus of paramount importance. Inorganic catalysts can be easier to recover, they present a high number of vicinal active sites, and their acidity is easily tuned.

Recently, some efforts have been done towards such achievement. Guo et al. firstly showed the possibility of a heterogeneous FLP on a gold surface.[3] The latter behaves as a Lewis acid when combined with imines and nitriles. DFT calculations highlighted that the "frustration" comes from the repulsion between the imine lone pair and the filled d-band of the gold surface. Experimentally, nitriles and imines were hydrogenated using a gold powder which is normally unreactive towards H_2 activation. Gold surfaces have been later studied also by Rossi et al., who described the cooperative activation of H_2 by a supported Au species in the presence of nitrogenous bases.[4] The latter are of paramount importance since they play a key role in the catalytic activity and selectivity. Such system was capable of hydrogenating alkynes to alkenes with high conversion and high *cis* selectivity whereas the gold is normally inactive. Lately, the same group reported an 'all heterogeneous' catalyst obtained by pyrolysis of gold acetate in the presence of 1,10-phenantroline and TiO_2.[5] This process led to Au nanoparticles (Nps) embedded in a nitrogen doped carbon/TiO_2 support active for the *cis* selective hydrogenation of alkynes into alkenes. DFT calculations strongly supported the hypothesis that a FLP interaction is responsible for the catalytic activity. In the field of all-solid heterogeneous FLP many advances have been made recently. Sheng Su et al. have reported a boron-nitrogen graphene catalyst capable of activating hydrogen in very mild conditions.[6] N-doped carbon was used by Li et al. to create Lewis acid-base pairs on the surface modified with Cu or Ni nanoparticles for CO_2 or methanol fixation, respectively.[7,8] Ozin et al. deeply studied Indium oxide/hydroxide mixtures clearly showing a FLP reactivi-

ty towards the activation of CO_2 and H_2.[9] While most of these systems work better in the light than in the dark, a careful selection of the right crystalline phase of a $In_2O_{3-x}(OH)_y$ nanomaterial leads to a highly active catalyst capable of activating H_2 at room temperature.[10] The activity of such systems derives from the surface defects in oxygen distribution which causes the formation of small reactive pockets. Such phenomenon has been recently exploited by Qu et al. who reported the spectacular reactivity of a CeO_2 catalyst for the hydrogenation of olefins.[11] Recently, the group of Ozin used copper substitution in calcium hydroxyapatite to design a CO_2 hydrogenation catalyst.[12] All these solid heterogeneous catalysts, however, do not take benefit from the mobility of a molecular partner in solution, which can greatly increase the chances of identifying novel FLPs systems.

In this context, we wanted to investigate the possibility of creating a FLP in colloidal solutions based on inorganic nanoparticles of abundant first row transition metals (the Lewis acid) and an external ligand (the Lewis base), free to come and go from the nanoparticle's surface. The use of first-row transition metals is nowadays becoming a major trend because of environmental, health and economic issues associated to the utilization of noble metals.[13] However, nanoparticles interaction with strong Lewis base may lead to undesired leaching effects, producing molecular species in solution, as identified recently on copper nanoparticles for instance.[14] For the present study, we selected nickel-cobalt nanoparticles, for which preliminary tests showed the absence of leaching. As a benchmark reaction, we selected the activation of Si–H bonds of silanes, which was easily followed by monitoring the silane consumption in the reaction medium by ^{1}H NMR, using mesitylene as an internal standard. In order to further drive the reaction, the silane was engaged in the hydrosilylation of aldehydes, forming the corresponding mono, bis, and tris-silylether in variable proportions.

The classical mechanism for hydrosilylation by late transition-metal complexes is the Chalk-Harrod mechanism,[15] which starts by the oxidative addition of the Si–H bond on the metal center. An analog surface organometallic path could be written, with the same starting elementary step, sensitive to the presence of nearby phosphines through steric and electronic effect. Such elementary step can hardly be monitored on the surface of a colloid, hence, the present study will not provide a final proof of reaction mechanism (surface organometallic *vs.* our proposition of a *NanoFLP*, depicted on **Figure 1** and commented below). Rather, we will investigate all the reaction parameters in order to assess the viability of the *NanoFLP* mechanism, as our main purpose is to introduce this concept in the nanocatalysis community. We will see below that few arguments may reinforce the proposed *NanoFLP* mechanism. We provide this analysis as an incentive for theoretical chemists to model the ligand-covered metal surface and weight the relative energy barrier of each path, and as another incentive to experimental chemists to use the Tolman cone angle as a key parameter for future reactions catalyzed by *NanoFLP*.

Amongst hydrosilanes, phenylsilane is considered as a strong hydride donor and thus an easy-to-activate molecule: it was selected for the first series of experiments (Table 1). Benzaldehyde was selected as a co-substrate and the reaction was performed at room temperature in THF during 24h. NiCo nanoparticles (NiCoNPs) of 12±1 nm diameter were prepared according to the literature (see ESI, for the synthesis protocol).[16] It should be noted that the nanoparticles were synthesized in the presence of tri-*n*-octylphosphine ($PnOct_3$) as a stabilizing agent. The phosphine was mostly washed away during the nanoparticles purification step (at ca 95 % based on XPS) and, compared with the amount of phosphine added during the catalytic experiment (10 mol% vs. the silane), its remaining amount was negligible.

We verified in a first set of experiments, that the reaction without catalyst (acid or base) did not yield any silane consumption (Table 1, entry **1**, and ESI Figure S5) and that the Lewis acid NiCoNps (10 mol%), without added phosphine, were not active (entry **2** and Figure S6). Moreover, the reaction conducted with 10 mol% of the Lewis base $PnBu_3$ did not yield any silane consumption (Table 1, entry **3** and Figure S7). In contrast, the reaction performed in the presence of both the acid (NiCoNPs) and the base ($PnBu_3$) yield a silane consumption of 77 % (Table 1, entry **4** and Figure S8). It was accompanied by the consumption of 0.5 equiv. of benzaldehyde, observed by the reduction of the integration value for the peak at 10.0 ppm, and the formation of the silylethers characterized by a peak at 4.8 ppm (Figure S8). Interestingly, the reaction was sensitive to the catalytic loading of NiCoNPs/$PnBu_3$: silane consumption dropped to 22 % when only 5 mol% of NiCoNPs/$PnBu_3$were used, and increased to 100 % with 20 mol% of NiCoNPs/$PnBu_3$ (Table 1, entry **5** and **6** respectively, and Figures S9 and S10, respectively). These first results were consistent with the idea that NiCoNPs and $PnBu_3$ were forming a FLP in solution, which was responsible for the room-temperature activation of the Si–H bond of the silane. However, at this stage, more classical effects such as the electronic effect of the phosphine on the NiCo surface, could not be discarded.

The formation of a FLP between a NiCo nanoparticle and a phosphine, which we will call here a *NanoFLP* depicted on **Figure 1E**, should depend both on the relative acidity of the nanoparticles and the ligand, and on the steric hindrance of the ligand, with some couples of partners optimal for some specific substrate. This rationale is directly extracted from well-established results for intermolecular FLPs in solution.[2] While the Lewis acidity evaluation of a metallic surface remains challenging, it is easy to play with the Lewis basicity and steric hindrance of phosphines. To appreciate this effect, we lowered back the catalytic charge to 10 mol%. Delightfully, changing the ligand greatly affected the catalytic activity, while the colloidal stability was not compromised. Longer alkyl chain phosphines such as tri-*n*-octylphosphine lead to a lower phenylsilane consumption (55%, Table 1 entry **7** and Figure S11), suggesting that a higher steric hindrance was detrimental to the reaction. As a matter of fact, more hindered tricyclohexylphosphine yielded even lower consumption (7%, Table 1 entry **8** and Figure S12). However, a much less hindered ligand such as trimethylphosphine was only poorly active, suggesting that a fine balance between the steric hindrance and the Lewis basicity is required to achieve an optimal catalytic activity (entry **9** and Figure S13).

We also investigated a series of arylphosphines: when triphenylphosphine was employed, 100% of phenylsilane consumption was achieved (Table 1 entry **10** and Figure S14). Following the Tolman classification,[17] PPh_3 should be slightly more hindered than $PnBu_3$ which might explain the enhanced catalytic activity. Accordingly, less hindered phosphines such as $PMePh_2$ and PMe_2Ph were less active (Table 1 entry **11** and **12** respectively and Figures S15 and S16, respectively). Furthermore, a bidentate ligand such 1,4-bis(diphenylphosphino)butane (dppb) was active reaching a phenylsilane consumption of 66%, while a tridentate ligand such as bis(diphenylphosphinoethyl)phenylphosphine (triphos) was totally inactive probably because of a too high steric hindrance (Table 1, entry **13** and entry **14** respectively and Figures S17 and S18, respectively).

Finally, the scope was extended to ligands other than phosphines. Triphenylphosphite, which is poorly hindered, showed 25 % silane consumption (entry **15** and Figure S19**)**. In relation with the work of van Leeuwen,[18] we also tested diphenylphosphine oxide, which yielded a low silane consumption of 5% (entry **16** and Figure S20).

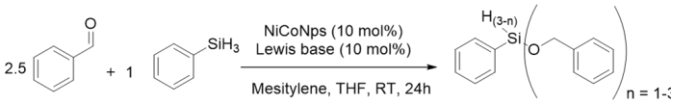

Entry	Lewis acid	Lewis base	Silane consumption[a]
1	-	-	0%
2	NiCoNps	-	0%
3	-	P*n*Bu$_3$	0%
4	NiCoNps	P*n*Bu$_3$	77%
5[b]	NiCoNps	P*n*Bu$_3$	22%
6[c]	NiCoNps	P*n*Bu$_3$	100%
7	NiCoNps	P*n*Oct$_3$	55%
8	NiCoNps	PCy$_3$	7%
9	NiCoNps	PMe$_3$	20%
10	NiCoNps	PPh$_3$	100%
11	NiCoNps	PPh$_2$Me	70%
12	NiCoNps	PPhMe$_2$	17%
13	NiCoNps	dppb	66%
14	NiCoNps	triphos	0%
15	NiCoNps	P(OPh)$_3$	25%
16	NiCoNps	HPPh$_2$O	5%

Table 1 Catalytic activity of different catalysts combined with different ligands. [a] Silane consumption is calculated by ^{1}H NMR using mesitylene as internal standard. [b] 5 mol% of NiCoNPs and Lewis base. [c] 20 mol% of NiCoNPs and Lewis base.

In order to assess the results in a more comprehensive approach, we investigated trends amongst sub-ensemble of phosphines, namely, the monodendate phosphines. We plotted the silane consumption as a function as the basicity of the phosphine, based on their pKa, for lack of a better parameter. Alkylphosphines pKa are spread on a small range of values, from 8.13 for P*n*Oct$_3$ (see Table S1) to 9.70 for PCy$_3$. **Figure 1**A shows that moderated pKa around 8.2-8.4 correspond to higher phenylsilane activation. A similar plot was made for arylphosphines on **Figure 1**B. In this case, no local optimum was observed and the most efficient reaction was obtained with the less basic phosphine of the series, PPh$_3$. So far, the pKa did not appear as a critical parameter explaining the activation of Si–H in phenylsilane. This result resonated with the study of Fiorio *et al.* on gold nanoparticles functionalized with amines, where no clear relation between the pKa and the catalytic activity was found.[4]

Then, we looked for a more relevant electronic parameter to describe the phosphine interaction with the metal. We selected the Tolman electronic parameter (TEP),[17] which is a semi-quantitative measure of the electron donating or withdrawing ability of a ligand. **Figure 1**C shows the two previous series of phosphines, as well as triphenylphosphite (in green). Once again, no clear trend was found since the best two phosphines for the reaction, P*n*Bu$_3$ and PPh$_3$, showed very different TEP of 2060.3 and 2068.9 cm^{-1}, respectively. This result is quite interesting to consider: in the framework of a surface organometallic mechanism, the reaction yield might have been more clearly correlated to the TEP.[19]

The steric hindrance should also play a major role on the ability of the phosphine to approach the surface while not forming a too strong adduct, thanks to the steric frustration. Thus, we plotted the same series of data vs. the Tolman cone angles[17] on **Figure 1**D. This cone angle is defined as the solid angle formed with the metal at the vertex, centered at a distance of 2.28 Å from the phosphorus and the van der Waals radii of the outermost atoms at the perimeter of the cone. Here, we observed that a common trend could explain the activity of alkylphosphines, arylphosphines and triphenylphosphite: phenylsilane was better activated by species with higher Tolman cone angles, to a certain limit. Above a cone angle of ca 155°, the phosphine probably did not approach the surface often enough, as seen with PCy$_3$ (170°). Interestingly, if the reaction was proceeding through a surface organometallic path, we might expect that the trend vs. the cone angle would be linear, as observed for Ni complexes (bulkier phosphine would be disfavored as they would hinder the oxidative addition step).[19] This does not correspond to the current observation of volcano shape. In our view, this trend linking the Tolman angle and the catalytic efficiency of the NiCoNPs/phosphine strongly suggested that the phosphine formed an encounter complex with the surface: it should be small enough to access it despite the presence of other ligands on the surface, but it should be large enough not to block the surface active sites by staying indefinitely on the surface. Such a fine balance between the Lewis basicity and the steric hindrance is typical of FLPs formed by two molecular partners,[20] which reinforces our proposition that NiCoNPs and PPh$_3$ are forming a *NanoFLP*.

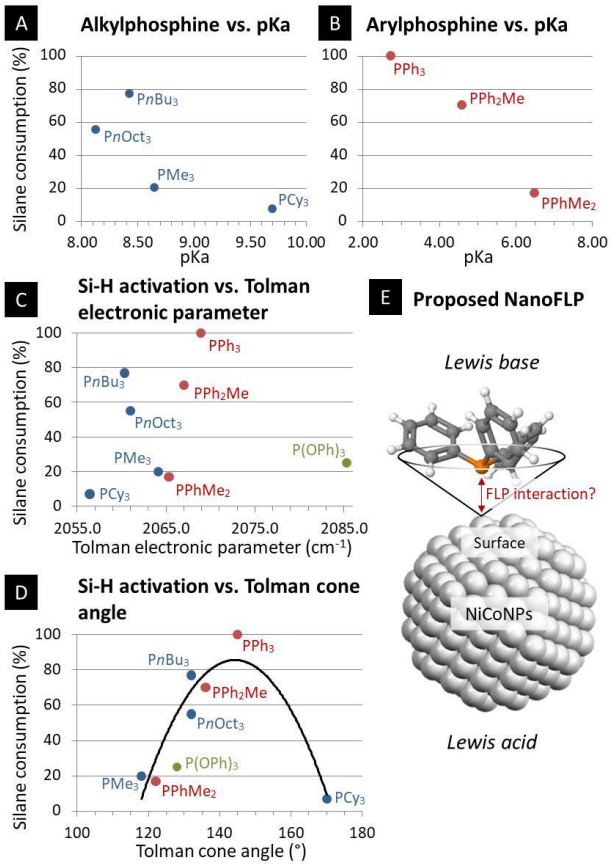

Figure 1 Silane consumption reported as a function of pKa for selected alkylphosphines (A) and arylphosphines (B). Silane consumption reported as a function of Tolman electronic parameter (C). Silane consumption reported as a function of Tolman cone angle (D), the black curve is the modeling of the trend by a polynome of degree 2, plotted as a guide to the eye. (E) Scheme of the envisioned *NanoFLP*, showing the phosphine interaction (here, PPh$_3$) with the nanoparticle surface. The Tolman cone angle is plotted as a guide to the eye.

As a complementary argument, it is relevant to compare the cases of PPh$_3$, dppb and triphos in order to assess the effect of multiple phosphine moieties: multidentate ligands typically reside for

longer time on a surface, once coordinated. Consumption of phenylsilane decreases within this series, suggesting once more that the residence time of the phosphine should probably not be too long for the catalytic NiCoNPs/phosphine couple to be active.

Overall, the results discussed so far can be summarized in two points: 1) the activation of the Si–H bond in phenylsilane is exclusively allowed by the combination of NiCoNPs and an adequate phosphine, 2) the catalytic activity strongly depends from the Tolman cone angle and the Lewis basicity of the phosphine.

Therefore, for a thorough understanding of such reactivity we decided to deeply study the most active catalytic couple: NiCoNps/PPh_3. Firstly, we investigated the kinetics of this transformation by recording the catalytic consumption of phenylsilane at two, four, eight, sixteen and twenty-four hours. We also took the occasion to explore the effect of different amount of ligand when a same catalytic loading of Nps is employed (**Figure 2**). Interestingly, when PPh_3 was lowered to 2.5 mol% no reactivity was observed, meaning that a minimum of phosphine is required to form the active species. As expected, with 5 mol% of phosphine, the reaction proceeded slower compared to the optimized conditions and the consumption did not reach 100 % after 24 h. When the optimal parameters were utilized (10 mol% of nanoparticles and of phosphine) we observed a rapid increase of phenylsilane consumption after 4 h and the reaction was already completed after 16 h. Interestingly, when a double amount of PPh_3 (20 mol%) was employed, the reaction was slightly slower compared to the optimized conditions.

This suggests that an optimal equilibrium between coordinated and non-coordinated Lewis base was reached when a 1:1 ratio of nanoparticles to phosphine was employed. Pushing the steady state toward more coordinated phosphine was detrimental to the activation of the Si–H bond. This result is consistent with the comparison made above between monodentate, bidentate and tridentate phenylphosphines.

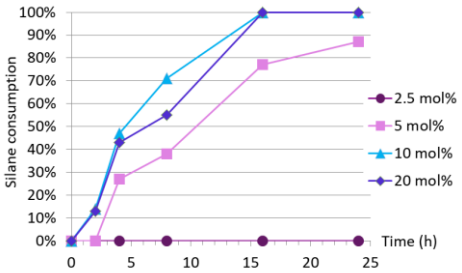

Figure 2 Kinetic study for the hydrosilylation of benzaldehyde using different amount of PPh_3.

In the framework of a surface organometallic mechanism, a metal-ligand ratio of 1:1 to 1:2 might be optimal (hence well below the introduced ratio 2.5 mol%), based on studies on nickel complexes. The current observation does not seem to concur,[19] although we are not able to characterize the proportion of free phosphine in solution under catalytic conditions. In the framework of the possible formation of a *NanoFLP*, we would expect the following: the phosphine is in exchange from the surface to the solution, but a too low concentration of the phosphine would make the formation of the intermediate species NiCoNps—Silane—PPh_3, where the Si–H bond of the silane is trapped in the reactive pocket of the FLP, unfavored. The concentrations corresponding to 2.5, 5, 10 and 20 mol% of PPh_3 were respectively 2, 4, 8 and 16 mmol/L.

Experimentally, free PPh_3 in solution was detected by ^{31}P NMR when used at 20 mol%. This confirmed that all the phosphine was not coordinated on the NiCoNPs surface. In order to get a clearer notion of the stoichiometry of PPh_3 vs. the number of surface atoms of the nanoparticles, a raw estimation was made, using the NiCoNPs average diameter and counting only the last layer of atoms. Roughly, for 10 mol% NiCoNPs, amounts of PPh_3 of 2.5, 5, 10 and 20 mol% correspond to 5, 10, 20 and 40 equiv. of phosphine vs. the surface atoms (see calculation in ESI section 10). The phosphine was always in large excess vs. the surface, which further emphasizes that the equilibrium with the free phosphine in solution was mandatory to insure that other substrate may access the surface. We however needed to finally exclude that such large amount of phosphine ligands were also generating molecular complexes in solution through a leaching process. Indeed, the leaching of molecular species is one of the most current issues in nanocatalysis. The latter can lead to a misrepresentation of the active species.

In order to verify the absence of leaching, we tested the activity of reaction supernatant, as depicted on Scheme S1 in ESI. More precisely, a reaction using the optimal conditions was started and stopped after 4 h when ca 50 % of phenylsilane consumption was reached. The mixture was then separated by centrifugation. The supernatant (containing silylethers, free PPh_3, as well as unreacted silane and benzaldehyde) was recovered, filtered using a syringe filter and further stirred for 4 h. No reaction was observed, indicating the absence of catalytic species in the supernatant. Alongside, the precipitate was also recovered and refilled with a fresh mixture containing all reagents of a standard reaction (namely, benzaldehyde and phenylsilane), but no PPh_3. Even in this case, after 4 h of stirring, no hydrosilylated products were observed. This indicated that NiCoNPs were not permanently activated prior to centrifugation (by surface reconstruction or other phenomena). Furthermore, to confirm the dynamic nature of the catalytic species we added one equivalent of PPh_3 to the latter mixture and stirred it for 16 h. As expected in the presence of both the NiCoNps and the phosphine, we observed significant phenylsilane consumption (70 %), confirming a regain of the catalytic activity. Besides, an aliquot of the NiCoNps was taken after the first 4 h-reaction and observed by TEM (Figure S2). The nanoparticles were identical in morphology to the fresh ones and showed no sign of leaching. Finally, to definitely exclude any homogeneous species, ICP-MS was performed on the supernatant isolated after 24 h of reaction. Nickel and cobalt contents were below the detection limit, confirming that no leaching was taking place. From these experiments, we can conclude that 1) the catalytic reaction happens at the surface of the NiCoNPs and 2) the phosphine plays an active role during the whole duration of the catalytic reaction, and not only at the beginning. While the first point confirms that we are performing nanocatalysis, the second supports once more that NiCoNps and PPh_3 could be forming a *NanoFLP*. As a complementary experiment, the activity of the nanoparticles was compared with these of $Ni(acac)_2$, with or without added phosphine (PPh_3 or P*n*Bu_3). Ni homogenous complexes are indeed also known as catalysts for hydrosilylation reactions.[21] The results showed on Table S3 show little dependence of the silane consumption to the presence of the phosphine. Moreover, the yield were of similar magnitude to these observed with NiCoNps, which suggests that the active species when using the nanoparticles should not be some sort of leached nickel at a concentration below the detection limit of the ICP-MS.

From this point, we investigated the nature of the NiCoNps/PPh_3 surface, and we assessed if it was evolving during the course of the reaction. Because the reaction was occurring at the interface between the nanoparticle and the solution, few tools were available for this investigation.

First, X-ray photoelectron spectroscopy (XPS) was used (**Figure 3**). We compared the spectra of the fresh NiCoNps with those of powders isolated after the optimized reaction (Table 1, **entry 10**),

indicated as "post mortem". We also analyzed fresh NiCoNps that were stirred in the presence of 1 equiv. of PPh_3, then washed and isolated, indicated as "blank". Overall, the Ni $2p_{3/2}$, Co $2p_{3/2}$, P2p and NiCo3P regions did not show strong differences between the three samples, meaning that the NiCoNPs surface was not significantly modified as a result of PPh_3 adsorption and of the catalytic reaction itself. In agreement with other works on NiCo,[16,22] the Ni $2p_{3/2}$ region was fitted with Ni(0) with the lower binding energy (B.E.) component at 852.7 eV (**Figure 3**A, in red) and a nickel oxidized species with the lower B.E. component at 854.7 eV (in blue), slightly higher in B.E. than NiO (expected at 853.7 eV).[23] The Co $2p_{3/2}$ region was fitted with a combination of Co(0) at 778.0 eV (**Figure 3**B, in red), a Co(II) species at 781.3 eV (in blue), slightly higher than the expected value for CoO (780 eV) and a third species at 780.7 eV (in green), slightly higher than the expected value for Co_3O_4 (779.6 eV).[24] The presence of metallic Ni (in red) and Co (in dark green) as major species was confirmed by analyzing the NiCo3p region (**Figure 3**D), fitted according to the literature.[22] The washing step of the nanoparticles, performed in air, should be responsible for part of the surface oxidation observed for all samples. Lastly, the P2p region (**Figure 3**C) showed the presence of phosphide species (in red, with a B.E. of 129.5 eV for the $P2p_{3/2}$ component), resulting from partial tri-*n*-octylphosphine decomposition during the formation of the nanoparticles.[16,25] At this stage of our study, it was not possible to determine if the phosphide presence significantly affect the reactivity of the NiCo surface. A second peak, broader, with $P2p_{3/2}$ at 130.7 eV (in green) was observed and attributed to phosphines adsorbed on Ni and Co sites: TOP[25] for fresh NPs (a) and likely PPh_3 for spectra (b) and (c).[26,27] The last peak with $P2p_{3/2}$ at 133.3 for spectrum (a) and 133.1 eV for spectra (b,c) (in blue) was attributed to tri-*n*-octylphosphine oxide and triphenylphosphine oxide, respectively. These species were likely formed as a result of air exposure prior to the XPS measurement.

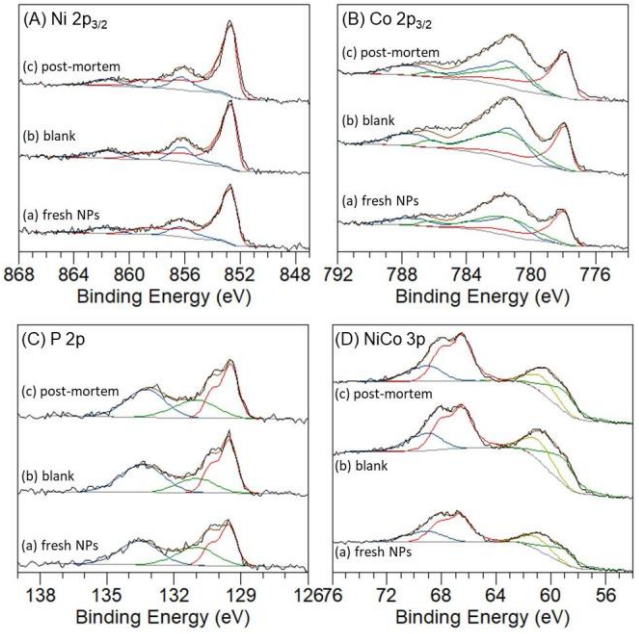

Figure 3 XPS of the (A) $Ni2p_{3/2}$, (B) $Co2p_{3/2}$, (C) P 2p and (D) NiCo3p regions for the NiCoNps (a) washed after synthesis, (b) exposed to PPh_3 and (c) collected at the end of the catalytic reaction. Ni2p was fitted with two sets of components: Ni(0) in red and NiO in blue. Co2p was fitted with three sets of components: Co(0) in red, CoO in blue and Co_3O_4 in green. P2p was fitted with three components: phosphide in red, adsorbed phosphine in green and phosphine oxide in blue. Co3p was fitted with two components: Co(0) in dark green and CoO_x in light green. Ni3p was fitted with two components: Ni(0) in red and NiO_x in blue.

Overall, XPS indicated the presence of metallic Ni and Co surface sites, available to coordinate phosphines. The surface was not significantly affected by the reaction. Moreover, the surface alloy may be key to adjust the Lewis acidity of the surface. Indeed, pure nickel nanoparticles were inactive in the reaction and pure cobalt nanoparticles were only poorly active (Table S2). Optimization of the Lewis acidity of the surface is, however, out of the scope of the present work.

The inelastic mean free path of photoelectrons is ca 10-12 Å for the Ni2p and Co2p regions and ca 19-20 Å for NiCo3p.[28] As a consequence, the deeper metal atoms of the NiCoNPs were not probed by this technique. In order to characterize the core of the nanoparticles, X-ray absorption at Ni and Co K-edges was performed in transmission mode. For this experiment, NiCoNps powders were isolated after 2, 4, 8, 16 and 24 hours of reaction performed under the optimized conditions (Table 1, entry **10**). X-ray absorption near edge structure (XANES) revealed that both nickel and cobalt were mostly metallic from the beginning to the end of the reaction (Figures S3 and S4). Ni edge was detected at 8831.6 eV, similar to the edge for the nickel foil (8831.6 eV). Co edge was detected at 7710.6 eV, close to the edge of the cobalt foil at 7710.8 eV. Most importantly, these spectra were identical to those of the native catalyst confirming that the nanoparticles structure was unaffected by the reaction. This result is consistent with observations made so far from XPS and with the leaching experiments.

We further investigated the relevance of $NiCoNPs/PPh_3$ as a *NanoFLP* by modifying the steric hindrance of the reaction substrate: the silane. Indeed, in the case of a true *NanoFLP*, we expected that a fine adjustment of the phosphine is required when changing the characteristic of the Si–H bond to activate. Thus, we performed the hydrosilylation of benzaldehyde using less reactive and bulkier silanes, with NiCoNps and phosphine presenting a wide range of Tolman angles: PMe_3, $PnBu_3$, PPh_3, PCy_3 with angles of 118, 132, 145 and 170°, respectively. The first line of Table 2 recalls the values already mentioned in Table 1 for phenylsilane. When diphenylsilane was used as hydride source, no conversion was observed with PPh_3 whereas PMe_3 and $PnBu_3$, presenting lower Tolman angles, yielded conversions of 14 and 33%, respectively (Table 2 Entry **2**). In the framework of the surface organometallic mechanism, we could have expected that the reaction occurs faster with the less hindered PMe_3 than with $PnBu_3$, as both have close TEP. In the framework of the NanoFLP mechanism, we can propose that diphenylsilane was too bulky for the Si–H bond to be activated within the $NiCoNPs/PPh_3$ reactive site. The less hindered pair $NiCoNPs/PnBu_3$ was able to accommodate diphenylsilane. On the other hand, and as expected, less active silanes such as triphenylsilane or alkyl ones such as triethylsilane and tetramethyldisiloxane were not consumed with any of the phosphines tested (Table 2 Entry **3**, **4** and **5** respectively). Though possible, conditions optimization for the activation of such silanes is out of the scope of this work. However, this limited scope once again proved the existence of an active species being strongly dependent from the steric environment.

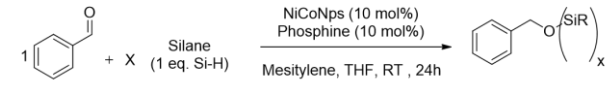

Entry	Silane	PMe_3 (118°)	$PnBu_3$ (132°)	PPh_3 (145°)	PCy_3 (170°)
1	Phenylsilane	20%	77%	100%	7%
2	Diphenylsilane	14%	33%	0%	0%
3	Triphenylsilane	0%	0%	0%	0%
4	Triethylsilane	0%	0%	0%	0%
5	Tetramethyldisiloxane	0%	0%	0%	0%

Table 2 Catalytic consumption of different silanes using NiCoNps and phosphines with a wide range of steric-hindrance (Tolman angles are indicated in parenthesis).

As a perspective, the hydrosilylation of other aldehydes with phenylsilane was attempted in the presence of NiCoNPs/PPh_3. Here, 1 equiv. of phenylsilane vs. the aldehyde was used. Thus, the conversion displayed herein is referred to the quantity of aldehyde transformed during the reaction. Interestingly, electron-poor benzaldehyde such as 4-nitrobenzaldehyde underwent hydrosilylation to a good extent while electron-rich 4-dimethylaminobenzaldehyde was less hydrosilylated (Figure 4 Entry **1** and **2** respectively). On the other hand, terephtalaldehyde and 3,4-dihydroxybenzaldehyde (Figure 4 Entry **3** and **4** respectively) were only poorly hydrosilylated. Such result is difficult to interpret but we may think that the presence of more coordinating sites is detrimental to the dynamic character of the active species and overall it inhibited the reaction. Additionally, alkylaldehydes such as *trans*-cynnamaldehyde and *trans*-2-octenal (Figure 4 Entry **5** and **6** respectively) were not hydrosilylated.

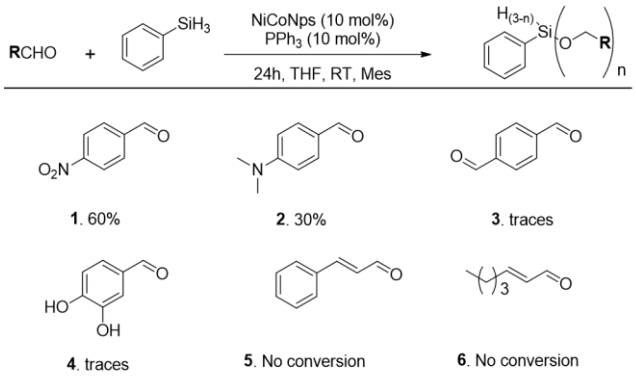

Figure 4 Hydrosilylation of aldehydes using the optimized conditions and one equivalent of phenylsilane. The conversion is calculated by NMR using mesitylene as internal standard.

In conclusion, this study reports the effect of phosphine on the activation of the Si–H bond of silanes by NiCoNps/phosphine during the hydrosilylation of benzaldehyde. The fact that the catalytic activity strongly depends from the steric hindrance and the Lewis basicity of the ligand, chosen from a series of commercially available phosphines, suggests that a Lewis interaction might be responsible for the observed reactivity. An empiric relation was found between the Tolman cone angle and the catalytic activity. Both indicate that the active sites on the NiCoNPs are strongly affected by the steric and electronic properties of the phosphine, consistent with the proposed model of a *NanoFLP* type of interaction. It is also shown that the phosphine mobility between the coordination site on the surface and the solution is essential to the activity, consistent with the proposed formation of an encounter complex as identified in some molecular FLPs. XANES and XPS analysis showed that the nanoparticles are mostly not affected by the reaction and the absence of leaching was verified.

The strong dependence of the reaction to the steric environment has been also demonstrated by changing the hydride source. With the bulkier diphenylsilane, a less bulky phosphine, PMe_3, was found to be more suitable for the reaction. This fine adjustment of the Lewis acid/base pairing in relation with the substrate bulkiness is also in line with trends found in molecular FLP chemistry. Organic ligands have been widely utilized to inhibit or 'poison' catalysts, especially in hydrogenation reactions. With this work we hope to prompt the way to a deeper consideration of the effect of organic ligands on metallic surface. While we do not finally discard the possibility of a classical oxidative addition on a bare metal center as the first elementary step (so-called surface organometallic mechanism), we propose here that the association of NiCoNPs and selected phosphines can be envisioned as a *NanoFLP* formed in the colloidal solution, where the Tolman angle is a key descriptor. Further proofs of this may come in future works by investigating the activation of other bonds, such as H–H, C=O, etc. and alternatively, by *in silico* modeling of the interactions involved in both mechanisms. Moreover, in-depth study of the ligand dynamics from the solution to the surface, in the presence or the absence of the reaction substrate, should be pursued for a better description of the catalytic species.

Experimental section

Reagents

Oleylamine (technical grade, 98%), Phenylsilane ($PhSiH_3$, 99%), benzaldehyde (BnzCHO, 99%), mesitylene (Mes, dried and degassed prior to utilization), tricyclohexylphosphine (PCy_3, 99%), trimethylphosphine (PMe_3, 99%), triphenylphosphine (PPh_3, 99%), diphenylmethylphosphine ($PMePh_2$, 99%), dimethylphenylphosphine (PMe_2Ph, 99%), diphenylphosphinobutane (dppb, 99%), bis(diphenylphosphinoethyl)phenylphosphine (triphos, 99%), triphenylphosphite ($POPh_3$, 99%), diphenylphosphine oxide ($HPPh_2O$, 99%), diphenylsilane (Ph_2SiH_2, 99%), triphenylsilane (Ph_3SiH, 99%), triethylsilane (Et_3SiH, 99%), tetramethyldisiloxane (TMDS, 99%) and anhydrous tetrahydrofuran (THF, 99.99%) were purchased from Sigma-Aldrich and stored in a glovebox. Tri-*n*-octylphosphine (TOP; 97%), tri-*n*-butyl phosphine ($PnBu_3$, 99%), dicobalt(0) octacarbonyl ($Co_2(CO)_8$; >95%), and nickel(II) acetylacetonate ($Ni(acac)_2$; anhydrous, min. 95%) were purchased from Strem Chemicals and stored in a glovebox (in the fridge for dicobalt octacarbonyl). All chemicals described above were used without further purification unless stated. Glassware was kept in an oven at 120 °C prior to utilization.

Catalytic reactions with phenylsilane and benzaldehyde

In the glovebox, benzaldehyde (1 mmol), phenylsilane (0.4 mmol), mesitylene (0.4 mmol) and THF (5 mL) are added to a 15 mL vial equipped with a magnetic stirrer and containing the catalyst (the catalytic charge is referred to the phenylsilane). The ligand is added and the mixture is let to stir the required amount of time in the glovebox. At the beginning of the reaction and after stirring, the nanoparticles are in a colloidal dispersion. At the end of the reaction the vial is taken out from the glovebox. A few nanoparticles stick to the stirring bar at this step, suggesting the presence of some aggregates for the larger colloids due to their magnetic properties. A drop of the solution is analyzed by NMR, the conversion is given as consumption of phenylsilane *vs* mesitylene.

Catalytic reactions with other silanes and benzaldehyde

In the glovebox, benzaldehyde (1 mmol), silane (1 eq. of Si–H), mesitylene (0.4 mmol) and THF (5 mL) are added to a 15 mL vial equipped with a magnetic stirrer and containing the catalyst (the catalytic charge is referred to the silane). The ligand is added and the mixture is let to stir for 24 h. At the end of the reaction the vial

is taken out from the glovebox and a drop is analyzed by NMR, the conversion is given as consumption of silane *vs* mesitylene.

Catalytic reactions with other aldehydes

In the glovebox, the required aldehyde (1 mmol), phenylsilane (0.4 mmol), mesitylene (0.4 mmol) and THF (5 mL) are added to a 15 mL vial equipped with a magnetic stirrer and containing the catalyst (the catalytic charge is referred to the phenylsilane). The ligand is added and the mixture is let to stir for 24h in the glovebox. At the end of the reaction the vial is taken out from the glovebox and a drop is analyzed by NMR, the conversion is given as consumption of benzaldehyde *vs* mesitylene.

ASSOCIATED CONTENT

Supporting Information

Procedure for the synthesis of nanoparticles, complementary catalytic experiments with Ni NPs, Co NPs, $Ni(acac)_2$, procedure for the leaching experiments, complementary analyses by NMR, XANES, IPC-MS and TEM, Tolman electronic parameter, cone angles and pKa of selected phosphines. The Supporting Information is available free of charge on the ACS Publications website.

AUTHOR INFORMATION

Corresponding Author

sophie.carenco@sorbonne-universite.fr

Notes

The authors declare no competing financial interests.

ACKNOWLEDGMENT

This project has received funding from the European Research Council (ERC) under the European Union's Horizon 2020 research and innovation programme (Grant agreement No. 758480). Sorbonne Université, CNRS and Collège de France are also acknowledged for support. We acknowledge the synchrotron SOLEIL for beamtime allocation on the SAMBA beamline (project 20191697) and the ROCK beamline (project 20201494). We acknowledge Antoine Miche from Sorbonne Université for the acquisition of the XPS spectra.

REFERENCES

(1) Stephan, D. W. Catalysis, FLPs, and Beyond. *Chem* **2020**, *6* (7), 1520–1526. https://doi.org/10.1016/j.chempr.2020.05.007.

(2) Rokob, T. A.; Hamza, A.; Pápai, I. Rationalizing the Reactivity of Frustrated Lewis Pairs: Thermodynamics of H 2 Activation and the Role of Acid−Base Properties. *J. Am. Chem. Soc.* **2009**, *131* (30), 10701–10710. https://doi.org/10.1021/ja903878z.

(3) Lu, G.; Zhang, P.; Sun, D.; Wang, L.; Zhou, K.; Wang, Z.-X.; Guo, G.-C. Gold Catalyzed Hydrogenations of Small Imines and Nitriles: Enhanced Reactivity of Au Surface toward H2via Collaboration with a Lewis Base. *Chem. Sci.* **2014**, *5* (3), 1082. https://doi.org/10.1039/c3sc52851k.

(4) Fiorio, J. L.; López, N.; Rossi, L. M. Gold-Ligand-Catalyzed Selective Hydrogenation of Alkynes into Cis-Alkenes via H2 Heterolytic Activation by Frustrated Lewis Pairs. *ACS Catal.* **2017**, *7* (4), 2973–2980. https://doi.org/10.1021/acscatal.6b03441.

(5) Fiorio, J. L.; Gonçalves, R. V.; Teixeira-Neto, E.; Ortuño, M. A.; López, N.; Rossi, L. M. Accessing Frustrated Lewis Pair Chemistry through Robust Gold@N-Doped Carbon for Selective Hydrogenation of Alkynes. *ACS Catal.* **2018**, *8* (4), 3516–3524. https://doi.org/10.1021/acscatal.8b00806.

(6) Sun, X. Y.; Li, B.; Liu, T. F.; Song, J.; Su, D. S. Designing Graphene as a New Frustrated Lewis Pair Catalyst for Hydrogen Activation by Co-Doping. *Phys. Chem. Chem. Phys.* **2016**, *18* (16), 11120–11124. https://doi.org/10.1039/c5cp07969a.

(7) Xue, Z.-H.; Han, J.-T.; Feng, W.-J.; Yu, Q.-Y.; Li, X.-H.; Antonietti, M.; Chen, J.-S. Tuning the Adsorption Energy of Methanol Molecules Along Ni-N-Doped Carbon Phase Boundaries by the Mott-Schottky Effect for Gas-Phase Methanol Dehydrogenation. *Angew. Chemie Int. Ed.* **2018**, *57* (10), 2697–2701. https://doi.org/10.1002/anie.201713429.

(8) Liu, Y.-X.; Wang, H.-H.; Zhao, T.-J.; Zhang, B.; Su, H.; Xue, Z.-H.; Li, X.-H.; Chen, J.-S. Schottky Barrier Induced Coupled Interface of Electron-Rich N-Doped Carbon and Electron-Deficient Cu: In-Built Lewis Acid–Base Pairs for Highly Efficient CO 2 Fixation. *J. Am. Chem. Soc.* **2019**, *141* (1), 38–41. https://doi.org/10.1021/jacs.8b08267.

(9) Ghuman, K. K.; Hoch, L. B.; Wood, T. E.; Mims, C.; Singh, C. V.; Ozin, G. A. Surface Analogues of Molecular Frustrated Lewis Pairs in Heterogeneous CO 2 Hydrogenation Catalysis. *ACS Catal.* **2016**, *6* (9), 5764–5770. https://doi.org/10.1021/acscatal.6b01015.

(10) Wang, L.; Yan, T.; Song, R.; Sun, W.; Dong, Y.; Guo, J.; Zhang, Z.; Wang, X.; Ozin, G. A. Room-Temperature Activation of H 2 by a Surface Frustrated Lewis Pair. *Angew. Chemie Int. Ed.* **2019**, *58* (28), 9501–9505. https://doi.org/10.1002/anie.201904568.

(11) Huang, Z. Q.; Liu, L. P.; Qi, S.; Zhang, S.; Qu, Y.; Chang, C. R. Understanding All-Solid Frustrated-Lewis-Pair Sites on CeO2 from Theoretical Perspectives. *ACS Catal.* **2018**, *8* (1), 546–554. https://doi.org/10.1021/acscatal.7b02732.

(12) Guo, J.; Liang, Y.; Song, R.; Loh, J. Y. Y.; Kherani, N. P.; Wang, W.; Kübel, C.; Dai, Y.; Wang, L.; Ozin, G. A. Construction of New Active Sites: Cu Substitution Enabled Surface Frustrated Lewis Pairs over Calcium Hydroxyapatite for CO 2 Hydrogenation. *Adv. Sci.* **2021**, 2101382. https://doi.org/10.1002/advs.202101382.

(13) Wang, D.; Astruc, D. The Recent Development of Efficient Earth-Abundant Transition-Metal Nanocatalysts. *Chem. Soc. Rev.* **2017**, *46* (3), 816–854. https://doi.org/10.1039/c6cs00629a.

(14) Frogneux, X.; Borondics, F.; Lefrançois, S.; D'Accriscio, F.; Sanchez, C.; Carenco, S. Surprisingly High Sensitivity of Copper Nanoparticles toward Coordinating Ligands: Consequences for the Hydride Reduction of Benzaldehyde. *Catal. Sci. Technol.* **2018**, *8* (19), 5073–5080. https://doi.org/10.1039/c8cy01516c.

(15) Chalk, A. J.; Harrod, J. F. Homogeneous Catalysis. II. The Mechanism of the Hydrosilation of Olefins Catalyzed by Group VIII Metal Complexes 1. *J. Am. Chem. Soc.* **1965**, *87* (1), 16–21. https://doi.org/10.1021/ja01079a004.

(16) Carenco, S.; Wu, C.-H.; Shavorskiy, A.; Alayoglu, S.; Somorjai, G. A.; Bluhm, H.; Salmeron, M. Synthesis and Structural Evolution of Nickel–Cobalt Nanoparticles Under H2 and CO2. *Small* **2015**, *11* (25), 3045–3053.

https://doi.org/10.1002/smll.201402795.

(17) Tolman, C. A. Steric Effects of Phosphorus Ligands in Organometallic Chemistry and Homogeneous Catalysis. *Chem. Rev.* **1977**, *77* (3), 313–348. https://doi.org/10.1021/cr60307a002.

(18) Cano, I.; Huertos, M. A.; Chapman, A. M.; Buntkowsky, G.; Gutmann, T.; Groszewicz, P. B.; Van Leeuwen, P. W. N. M. N. M. Air-Stable Gold Nanoparticles Ligated by Secondary Phosphine Oxides as Catalyst for the Chemoselective Hydrogenation of Substituted Aldehydes: A Remarkable Ligand Effect. *J. Am. Chem. Soc.* **2015**, *137* (24), 7718–7727. https://doi.org/10.1021/jacs.5b02802.

(19) Bartik, T.; Nagy, G.; Kvintovics, P.; Happ, B. Steuerung Der Nickel(O)-Katalysierten Hydrosilylierung von Phenylacetylen Mit Phosphorliganden. *J. Organomet. Chem.* **1993**, *453* (1), 29–32. https://doi.org/10.1016/0022-328X(93)80323-4.

(20) Rokob, T. A.; Hamza, A.; Stirling, A.; Soós, T.; Pápai, I. Turning Frustration into Bond Activation: A Theoretical Mechanistic Study on Heterolytic Hydrogen Splitting by Frustrated Lewis Pairs. *Angew. Chemie Int. Ed.* **2008**, *47* (13), 2435–2438. https://doi.org/10.1002/anie.200705586.

(21) Zheng, J.; Darcel, C.; Sortais, J.-B. A Convenient Nickel-Catalysed Hydrosilylation of Carbonyl Derivatives. *Catal. Sci. Technol.* **2013**, *3* (1), 81–84. https://doi.org/10.1039/C2CY20509B.

(22) Bonifacio, C. S.; Carenco, S.; Wu, C. H.; House, S. D.; Bluhm, H.; Yang, J. C. Thermal Stability of Core-Shell Nanoparticles: A Combined in Situ Study by XPS and TEM. *Chem. Mater.* **2015**, *27* (20), 6960–6968. https://doi.org/10.1021/acs.chemmater.5b01862.

(23) Mansour, A. N. Characterization of NiO by XPS. *Surf. Sci. Spectra* **2002**, *3* (3), 231–238. https://doi.org/10.1116/1.1247751.

(24) Biesinger, M. C.; Payne, B. P.; Grosvenor, A. P.; Lau, L. W. M.; Gerson, A. R.; Smart, R. S. C. Resolving Surface Chemical States in XPS Analysis of First Row Transition Metals, Oxides and Hydroxides: Cr, Mn, Fe, Co and Ni. *Appl. Surf. Sci.* **2011**, *257* (7), 2717–2730. https://doi.org/10.1016/j.apsusc.2010.10.051.

(25) Carenco, S.; Liu, Z.; Salmeron, M. The Birth of Nickel Phosphide Catalysts: Monitoring Phosphorus Insertion into Nickel. *ChemCatChem* **2017**, *9* (12), 2318–2323. https://doi.org/10.1002/cctc.201601526.

(26) Blackburn, J. R.; Nordberg, R.; Stevie, F.; Albridge, R. G.; Jones, M. M. Photoelectron Spectroscopy of Coordination Compounds. Triphenylphosphine and Its Complexes. *Inorg. Chem.* **1970**, *9* (10), 2374–2376. https://doi.org/10.1021/ic50092a039.

(27) K. Kouba, J.; Pierce, J. L.; Walton, R. A. X-Ray Photoelectron Spectra of Inorganic Molecules XXlX. The Characterization of Mixed Phosphido-Phosphine and Phosphido-Phosphite Complexes of Transition Metal Carbonyl Clusters Using X-Ray Photoelectron Spectroscopy. *J. Organomet. Chem.* **1980**, *202* (4), C105–C107. https://doi.org/10.1016/S0022-328X(00)81880-X.

(28) Tanuma, S.; Powell, C. J.; Penn, D. R. Calculation of Electron Inelastic Mean Free Paths (IMFPs) VII. Reliability of the TPP-2M IMFP Predictive Equation. *Surf. Interface Anal.* **2003**, *35* (3), 268–275. https://doi.org/10.1002/sia.1526.

Table of Contents artwork